MATCH
Communications in Mathematical and in Computer Chemistry

MATCH Commun. Math. Comput. Chem. **90** (2023) 581–607
ISSN: 0340–6253
doi: 10.46793/match.90-3.581C

Hopf Bifurcation and Self–Organization Pattern of a Modified Brusselator Model

Mengxin Chen*

College of Mathematics and Information Science, Henan Normal University, Xinxiang 453007, China

chmxdc@163.com

(Received April 6, 2023)

Abstract

This paper reports the Hopf bifurcation and self-organization pattern of a modified Brusselator model. The model is a non-standard Brusselator model, it involves the nonlinear restraint term. For the non-diffusive model, we give the types of unique positive equilibrium. It is found that the unique positive equilibrium may be focus, node, or center and we establish their stability, respectively. Especially, there exists the spatial homogeneous Hopf bifurcation when the equilibrium is a center. The first Lyapunov number technique is applied to perform the direction of the spatial homogeneous Hopf bifurcation. In the sequel, the occurrence conditions of the Turing instability and the spatial inhomogeneous Hopf bifurcation are given for the diffusive model. Moreover, by using the normal form theory, we show that the Hopf bifurcation is supercritical or subcritical. Finally, the self-organization patterns induced by the Turing instability and periodic solutions resulting from the Hopf bifurcation are displayed by employing numerical simulations. Our theoretical predictions and numerical results reveal that the modified Brusselator model enjoys the temporal period oscillation and spatial oscillation due to the Hopf bifurcation and Turing instability, respectively. These results may help us to figure out the spatio-temporal dynamics of such modified Brusselator model.

*Corresponding author.

1 Introduction

Various chemical models are usually used to investigate the self-organization pattern due to the interactions between the reactants. Pattern phenomenon is a vital aspect to understand the spatial dynamic profiles of the chemical models. Generally, the models involve the diffusion effect since the random movements of the reactants. Nowadays, there are many existing results that report the self-organization pattern of diffusive chemical models. Asheghi [1] given the influence of the diffusion coefficient of the homogeneous steady state and obtained the direction of the Hopf bifurcation by investigating a reduced Gierer-Meinhardt model. Chen and Wang [2] reported the boundedness of the solution and studied the properties of the Hopf bifurcation for a generalized Lengyel-Epstein model. Muntari and Sengül [3] performed a rigorous characterization of the types and structure of the dynamic transitions and showed the relation between the dynamic transitions and the pattern formations of a Brusselator model in a 2D rectangular box. Wong and Ward [4] developed a hybrid asymptotic-numerical theory with respect to the effect of different types of localized heterogeneities on the existence, stability, and slow dynamics of spot patterns for the Schnakenberg reaction-diffusion model in a 2-D domain. Please refer to [5–9] for more dynamic results with respect to the chemical models.

In this paper, we are especially interested in the bifurcation and self-organization pattern of the Brusselator model. As usual, this model follows the reaction steps

$$A \longrightarrow U,\ B+U \longrightarrow V+D,\ 2U+V \longrightarrow 3U,\ U \longrightarrow E,$$

where A, B, D, E, U and V are chemical reactants or products. Accordingly, Prigogene and Lefever in [10] built the following diffusive version Brusselator model

$$\begin{cases} \frac{\partial U}{\partial T} = D_1 \Delta U + A - (B+1)U + U^2 V, \\ \frac{\partial V}{\partial T} = D_2 \Delta V + BU - U^2 V, \end{cases} \tag{1}$$

where D_1 and D_2 are two positive constants and describe the diffusion

rates of two intermediary reactants $U(X,T)$ and $V(X,T)$ at time T and location X, respectively; A and B are two positive constants in the model and Δ is the Laplacian operator. Now setting

$$t = T,\ d_1 = D_1,\ d_2 = D_2,\ a = A,\ \gamma = B,\ u = U,\ v = V,$$

and introducing $\bar{u} = u/a, \bar{v} = av/\gamma$. Then if we drop the headlines, the following model is obtained.

$$\begin{cases} \frac{\partial u}{\partial t} = d_1\Delta u + 1 - (\gamma+1)u + \gamma u^2 v, \\ \frac{\partial v}{\partial t} = d_2\Delta v + bu - bu^2 v, \end{cases} \tag{2}$$

where we set $b = a^2$, parameters d_1, d_2, b, γ are positive constants and the nonlinear term u^2v describe the autocatalytic step. We need to mention that model (2) is a standard Brusselator equation, and it has attracted many scholars to investigate the various dynamic phenomena, see Refs. [11–14] and the reference cited therein. Note that the concentration of reactants will affect the reaction process and the production of reaction products. Thereby, if we suppose the autocatalytic step is a shorter term, namely, one replaces the term u^2v by nonlinear restraint term $\frac{u^2v}{1+u}$ in the model (2), this gives the following modified Brusselator model

$$\begin{cases} \frac{\partial u}{\partial t} = d_1\Delta u + 1 - (\gamma+1)u + \frac{\gamma u^2 v}{1+u}, & x \in \Omega, \quad t > 0, \\ \frac{\partial v}{\partial t} = d_2\Delta v + bu - \frac{bu^2 v}{1+u}, & x \in \Omega, \quad t > 0, \\ \frac{\partial u}{\partial \nu} = \frac{\partial v}{\partial \nu} = 0, & x \in \partial\Omega, \quad t \geq 0, \\ u(x,0) = u_0(x) \geq 0, \quad v(x,0) = v_0(x) \geq 0, & x \in \Omega, \end{cases} \tag{3}$$

where $\Omega \subset \mathbb{R}^N$ is a bounded domain for $N \geq 1$, ν is the outward unit normal vector along the smooth boundary $\partial\Omega$; $u_0(x) \geq 0$ and $v_0(x) \geq 0$ imply that the initial concentrations of two intermediary reactants u and v, respectively. If the diffusion effect is absent, we get the following spatial homogeneous modified Brusselator model:

$$\begin{cases} \frac{du}{dt} = 1 - (\gamma+1)u + \frac{\gamma u^2 v}{1+u}, \\ \frac{dv}{dt} = bu\left(1 - \frac{uv}{1+u}\right). \end{cases} \tag{4}$$

In this paper, we mainly focus on the dynamic profiles of the modified Brusselator model (3) and its local spatial homogeneous model (4) around the equilibrium E_*. Now an easy computation shows that $E_* = (1, 2)$ is a unique positive equilibrium of the model (3) and (4). Obviously, it is independent of the parameters b and γ. However, we can find some interesting phenomena by investigating the types of E_* based on the homogeneous model (4). To be exact, we have that (1) If $0 < \gamma \leq b + 2 - 2\sqrt{2b}$ or $\gamma \geq b + 2 + 2\sqrt{2b}$, then E_* is a node. (2) If $b + 2 - 2\sqrt{2b} < \gamma < b + 2$ or $b + 2 < \gamma < b + 2 + 2\sqrt{2b}$, then E_* is a focus. (3) If $\gamma = b + 2$, then E_* is a center, and there is the spatial homogeneous Hopf bifurcation for all $b > 0$. Of course, we perform the stability of the equilibrium E_* and give the direction of the Hopf bifurcation by using the first Lyapunov number [15]. For the diffusive model (3), we respectively give the occurrence conditions of the Turing instability and the spatial inhomogeneous Hopf bifurcation by treating γ as the critical parameter. In the sequel, we can illustrate that the modified Brusselator model (3) admits the supercritical or subcritical Hopf bifurcation with the help of the center manifold reduction and normal form theory [16–20]. In this fashion, we can ensure that the stability of the periodic solution resulted from the Hopf bifurcation. Finally, we present the self-organization pattern of the Brusselator model (3) around the Turing instability onset by employing numerical experiments. We conclude that the Brusseletor model with nonlinear restraint term could exhibit wealthy temporal and spatial dynamic behaviours. To summarize, our main contributions of the paper are as follows.

(1) The detailed classification conditions of the unique positive equilibrium are performed.

(2) We provide the exact formulas to determine the directions of the Hopf bifurcation so that we can ensure the stability of the periodic solutions.

(3) Complicated self-organization patterns are observed around the Turing instability threshold.

This paper is structured as follows. In Sec. 2, the stability of the positive equilibrium E_* and homogeneous Hopf bifurcation of the local model (4) are reported. In Sec. 3, we perform the occurrence conditions of the

Turing instability and Hopf bifurcation. Also, we investigate the direction of the Hopf bifurcation. In Sec. 4, we conduct numerical simulations to confirm the validity of the theoretical analysis. Some conclusions are made in Sec. 5.

2 Stability and Hopf bifurcation of (4)

Define $f(u,v) = 1-(\gamma+1)u+\frac{\gamma u^2 v}{1+u}$ and $g(u,v) = bu - \frac{bu^2 v}{1+u}$. Throughout a direct computation, we can find that model (4) has a unique positive equilibrium $E_* = (1,2)$ by setting $f(u,v) = g(u,v) = 0$.

Around the unique positive equilibrium $E_* = (1,2)$, we can determine the Jacobian matrix as below

$$J_0 = \begin{pmatrix} \frac{\gamma}{2}-1 & \frac{\gamma}{2} \\ -\frac{b}{2} & -\frac{b}{2} \end{pmatrix}.$$

As a consequence, the characteristic equation is given by

$$\lambda^2 - T_0(\gamma)\lambda + D_0(\gamma) = 0, \tag{5}$$

where $T_0(\gamma) = \frac{\gamma}{2} - \frac{b}{2} - 1, D_0(\gamma) = \frac{b}{2} > 0$. To perform the stability of the positive equilibrium E_*, we introduce $H(\gamma) = T_0^2(\gamma) - 4D_0(\gamma)$. A direct calculation shows that

$$H(\gamma) = \frac{1}{4}\gamma^2 - \frac{b+2}{2}\gamma + \frac{(b-2)^2}{4}.$$

Obviously, $H(\gamma) = 0$ must has two real roots, say γ_1 and γ_2, where

$$\gamma_1 = b+2-2\sqrt{2b} > 0, \qquad \gamma_2 = b+2+2\sqrt{2b} > 0.$$

Accordingly, we claim that $H(\gamma) \geq 0$ when $0 < \gamma \leq \gamma_1$ or $\gamma \geq \gamma_2$. Moreover, $H(\gamma) < 0$ if $\gamma_1 < \gamma < \gamma_2$ is valid. Now if $0 < \gamma \leq \gamma_1$ holds, namely, $0 < \gamma \leq b+2-2\sqrt{2b}$, we infer that $-\frac{b}{2} - 1 < \frac{\gamma}{2} - \frac{b}{2} - 1 \leq -\sqrt{2b}$. This gives that $T_0(\gamma) = \frac{\gamma}{2} - \frac{b}{2} - 1 < 0$ is valid. Consequently, the unique positive equilibrium E_* is a node, and it is locally asymptotically stable. Next if $b+2-2\sqrt{2b} < \gamma < b+2$ is valid, we immediately have $H(\gamma) < 0$ and

$-\sqrt{2b} < \frac{\gamma}{2} - \frac{b}{2} - 1 = T_0(\gamma) < 0$. As a result, the unique positive equilibrium E_* is a focus, and it is locally asymptotically stable. Now for the case $b+2 < \gamma < b+2+2\sqrt{2b}$, we deduce that $0 < \frac{\gamma}{2} - \frac{b}{2} - 1 = T_0(\gamma) \leq \sqrt{2b}$ and $H(\gamma) < 0$ are true. Thereby, the unique positive equilibrium E_* is a focus, and it is unstable. If $\gamma \geq \gamma_2$ holds, i.e., $\gamma \geq b+2+2\sqrt{2b}$, one yields $\frac{\gamma}{2} - \frac{b}{2} - 1 \geq \sqrt{2b} > 0$. This means that $T_0(\gamma) = \frac{\gamma}{2} - \frac{b}{2} - 1 > 0$ and $H(\gamma) > 0$. As such, the unique positive equilibrium E_* is a node, and it is unstable. Finally, if $\gamma = b + 2$, then it is easy to compute that the characteristic equation (5) has a pair of purely imaginary roots $\lambda = \pm i\sqrt{\frac{b}{2}}$. Hence, we claim that E_* is a center. In addition, if we denote by $\gamma_0^H = b + 2$ and suppose that $\lambda = \alpha(\gamma) \pm i\omega(\gamma)$ are the eigenvalues of the characteristic equation (5), then we can determine

$$\alpha(\gamma) = \frac{\gamma}{4} - \frac{b}{4} - \frac{1}{2}, \quad \omega(\gamma) = \frac{\sqrt{2b - \left(\frac{\gamma}{2} - \frac{b}{2} - 1\right)^2}}{2}. \tag{6}$$

Therefore, we can check that $\alpha(\gamma_0^H) = 0$ and $\omega(\gamma_0^H) = \sqrt{\frac{b}{2}} > 0$. In addition, one obtains $\alpha'(\gamma)|_{\gamma=\gamma_0^H} = \frac{1}{4} > 0$. Benefiting from the Poincaré Andronov-Hopf bifurcation theory, we know that model (4) undergoes the spatial homogeneous Hopf bifurcation at E_* when $\gamma = \gamma_0^H$.

To summarize the above analysis, we build the following stability result.

Theorem 1. *For the positive equilibrium $E_* = (1, 2)$ of the model (4), we have the following.*

(1) If $0 < \gamma \leq b + 2 - 2\sqrt{2b}$, then E_* is a node and it is locally asymptotically stable;

(2) If $b + 2 - 2\sqrt{2b} < \gamma < b + 2$, then E_* is a focus and it is locally asymptotically stable;

(3) If $b + 2 < \gamma < b + 2 + 2\sqrt{2b}$, then E_* is a focus and it is unstable;

(4) If $\gamma \geq b + 2 + 2\sqrt{2b}$, then E_* is a node and it is unstable;

(5) If $\gamma = b + 2$, then E_* is a center, and there is the spatial homogeneous Hopf bifurcation.

The following result concerns the direction of the Hopf bifurcation.

Theorem 2. *If $\gamma = \gamma_0^H = b+2$, then the direction of the Hopf bifurcation*

is supercritical.

Proof. Let $\check{u} = u - \frac{1}{\beta}, \check{v} = v - \frac{1}{\beta^2}$ and still denote $\check{u}, \check{v}$ by u, v, respectively. Then we obtain

$$\begin{cases} \frac{du}{dt} = & a_{10}u + a_{01}v + a_{20}u^2 + a_{11}uv + a_{02}v^2 + a_{30}u^3 + a_{21}u^2v \\ & +a_{12}uv^2 + a_{03}v^3 + \mathcal{O}(|u,v|^4), \\ \frac{dv}{dt} = & b_{10}u + b_{01}v + b_{20}u^2 + b_{11}uv + b_{02}v^2 + b_{30}u^3 + b_{21}u^2v \\ & +b_{12}uv^2 + b_{03}v^3 + \mathcal{O}(|u,v|^4), \end{cases} \tag{7}$$

where $\mathcal{O}(|u,v|^4)$ are higher terms and

$$\begin{aligned} &a_{10} = \frac{\gamma}{2} - 1, \quad a_{01} = \frac{\gamma}{2}, \quad a_{20} = \frac{\gamma}{4}, \quad a_{11} = \frac{3\gamma}{4}, \\ &a_{02} = 0, \quad a_{30} = -\frac{\gamma}{8}, \quad a_{21} = \frac{\gamma}{8}, \quad a_{03} = 0, \quad a_{12} = 0, \\ &b_{10} = -\frac{b}{2}, \quad b_{01} = -\frac{b}{2}, \quad b_{20} = -\frac{b}{4}, \quad b_{11} = -\frac{3b}{4}, \\ &b_{02} = 0, \quad b_{30} = \frac{b}{8}, \quad b_{12} = 0, \quad b_{21} = -\frac{b}{8}, \quad b_{03} = 0. \end{aligned}$$

From [15], we yield

$$\begin{aligned} L_1 =& \frac{-3\pi}{2a_{01}\mathrm{D}_0(\gamma)^{3/2}}\{[a_{10}b_{10}(a_{11}^2 + a_{11}b_{02} + a_{02}b_{11}) \\ &+ a_{10}a_{01}(b_{11}^2 + a_{20}b_{11} + a_{11}b_{02}) + b_{10}^2(a_{11}a_{02} + 2a_{02}b_{02}) \\ &- 2a_{10}b_{10}(b_{02}^2 - a_{20}a_{02}) - 2a_{10}a_{01}(a_{20}^2 - b_{20}b_{02}) \\ &- a_{01}^2(2b_{20}a_{20} + b_{11}b_{20}) + (a_{01}b_{10} - 2a_{10}^2)(b_{11}b_{02} - a_{11}a_{20})] \\ &- (a_{10}^2 + a_{01}b_{10})[3(b_{10}b_{03} - a_{01}a_{30}) + 2a_{10}(a_{21} + b_{12}) \\ &+ (b_{10}a_{12} - a_{01}b_{21})]\} \\ =& \frac{-3\pi}{2a_{01}\mathrm{D}_0(\gamma)^{3/2}}\{[a_{10}b_{10}a_{11}^2 + a_{10}a_{01}(b_{11}^2 + a_{20}b_{11}) \\ &- 2a_{10}a_{01}a_{20}^2 - a_{01}^2(2b_{20}a_{20} + b_{11}b_{20}) + (a_{01}b_{10} - 2a_{10}^2) \\ &\times (-a_{11}a_{20})] - (a_{10}^2 + a_{01}b_{10})(-3a_{01}a_{30} + 2a_{10}a_{21} - a_{01}b_{21})\} \\ =& \frac{-3\pi}{2a_{01}\mathrm{D}_0(\gamma)^{3/2}}\{[\frac{9b\gamma^2}{32} - \frac{9b\gamma^3}{64} + \frac{9b^2\gamma^2}{64} - \frac{3b\gamma^3}{64} - \frac{9b^2\gamma}{32} + \frac{3b\gamma^2}{32} \\ &+ \frac{\gamma^3}{16} - \frac{\gamma^4}{32} + \frac{b\gamma^3}{32} - \frac{3b^2\gamma^2}{64} + \frac{3b\gamma^3}{64} + \frac{3\gamma^4}{32} - \frac{3\gamma^3}{8} + \frac{3\gamma^2}{8}] \end{aligned}$$

$$
\begin{aligned}
&-\frac{5\gamma^4}{64}+\frac{3\gamma^3}{8}+\frac{b\gamma^3}{16}+\frac{b^2\gamma^2}{64}-\frac{9\gamma^2}{16}+\frac{\gamma}{4}-\frac{b\gamma}{16}\Big\}\\
=&\frac{-3\pi}{\mathrm{D}_0(\gamma)^{3/2}}\left\{\frac{3b\gamma}{8}-\frac{3b\gamma^2}{64}+\frac{7b^2\gamma}{64}-\frac{9b^2}{32}+\frac{\gamma^2}{16}-\frac{\gamma^3}{64}-\frac{3\gamma}{16}+\frac{1}{4}-\frac{b}{16}\right\}\\
=&\frac{-3\pi}{64\mathrm{D}_0(\gamma)^{3/2}}\left\{(24b+7b^2-12)\gamma-\gamma^3+(4-3b)\gamma^2-18b^2-4b+16\right\}.
\end{aligned}
$$

Consequently, around the spatial homogeneous Hopf bifurcation threshold $\gamma=\gamma_0^H=b+2$, we get the first Lyapunov number

$$L_1=\frac{-9\pi b(b^2+2b+8)}{64\mathrm{D}_0\left(\gamma_0^H\right)^{3/2}}<0.$$

Thereby, the Hopf bifurcation is supercritical and the periodic solution bifurcated from the Hopf bifurcation is stable. The proof is completed.

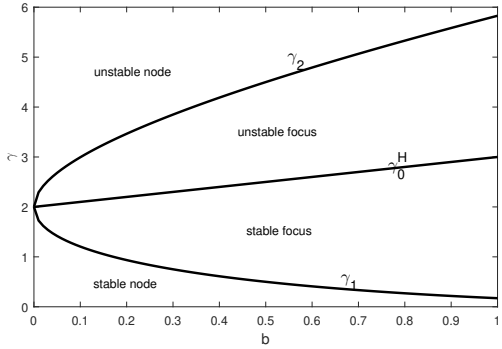

Figure 1. Stability domains of the unique positive equilibrium E_* in the plane of $b-\gamma$.

Remark 1. Figure 1 illustrates the stability domains of the unique positive equilibrium E_* in $b-\gamma$ plane. It is demonstrated that there are four domains, namely, stable node/focus domains and unstable node/focus domains.

Remark 2. In order to confirm the validity of some stability conclusions performed in Theorem 1, we display some phase portraits of the model (4) by using the ode45 numerical scheme. Treating $b=0.5$, then one has $\gamma_1=b+2-2\sqrt{2b}=0.5$ and $b+2=2.5$. Now we choose $\gamma=0.35\in(0,0.5)$.

It is found that the unique positive equilibrium $E_* = (1, 2)$ is a node, and it is stable, see Fig. 2(a). When taking $\gamma = 1.8 \in (0.5, 2.5)$, our numerical experiment shows $E_* = (1, 2)$ is a stable focus, see Fig. 2(b). In what follows, let us set $b = 3$, then we have $\gamma_1 = b + 2 - 2\sqrt{2b} = 0.1010$ and $b + 2 = 5$. Taking $3.5 = \gamma \in (0.1010, 5)$, then we claim that the unique positive equilibrium $E_* = (1, 2)$ is a stable focus, see Fig. 2(c). Finally, let us set $b = 1$, then we have $\gamma_1 = b + 2 - 2\sqrt{2b} = 1.1716$ and $b + 2 = 3$. Taking $2.5 = \gamma \in (0.1716, 3)$, then one declares that the unique positive equilibrium $E_* = (1, 2)$ is a stable focus, see Fig. 2(d). Thereby, conclusions (1) and (2) are valid.

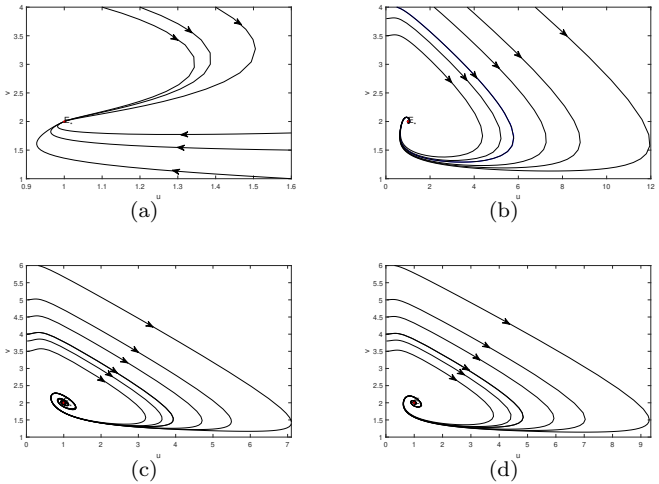

Figure 2. The phase portraits of model (4). (a): $E_* = (1, 2)$ is a stable node with $b = 0.5$ and $\gamma = 0.35 \in (0, 0.5)$; (b): $E_* = (1, 2)$ is a stable focus with $b = 0.5$ and $\gamma = 1.8 \in (0.5, 2.5)$; (c): $E_* = (1, 2)$ is a stable focus with $b = 2$ and $3.5 = \gamma \in (0, 4)$; (d): $E_* = (1, 2)$ is a stable focus with $b = 1$ and $2.5 = \gamma \in (0, 3)$.

Remark 3. Benefiting from Theorem 2, we know that model (4) undergoes the spatial homogeneous Hopf bifurcation and the periodic solution bifurcated from the Hopf bifurcation is stable around the threshold $\gamma = \gamma_0^H = b + 2$. As a result, we want to display the stable periodic solution through numerical experiments. Firstly, let us fix $b = 0.5$, then we

get $\gamma_0^H = 2.5$. Our numerical simulation shows there is the stable periodic solution, see Fig. 3(a). Fig. 3(b) displays the stable periodic solution near the Hopf bifurcation point $\gamma_0^H = 3.5$ with $b = 1.5$.

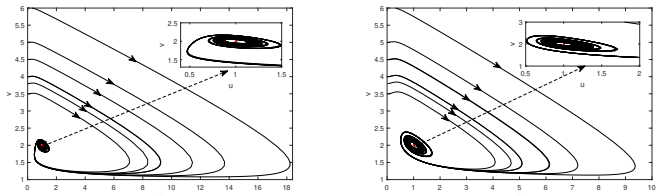

Figure 3. There are stable periodic solutions bifurcated from the Hopf bifurcation. (a): $b = 0.5$ and $\gamma = 2.5$; (b): $b = 1.5$ and $\gamma = 3.5$.

3 Turing instability and Hopf bifurcation of the diffusive model (3)

Near the unique positive equilibrium E_*, the linearization system of (3) has the form

$$\begin{cases} \frac{\partial u}{\partial t} \approx d_1 \Delta u + \left(\frac{\gamma}{2} - 1\right) u + \frac{\gamma}{2} v, & x \in \Omega, \quad t > 0, \\ \frac{\partial v}{\partial t} \approx d_2 \Delta v - \frac{b}{2} u - \frac{b}{2} v, & x \in \Omega, \quad t > 0, \\ \frac{\partial u}{\partial \nu} = \frac{\partial v}{\partial \nu} = 0, & x \in \partial\Omega, \quad t \geq 0, \\ u(x,0) = u_0(x) \geq 0, \quad v(x,0) = v_0(x) \geq 0, & x \in \Omega. \end{cases}$$

This is

$$\begin{pmatrix} u_t \\ v_t \end{pmatrix} = L \begin{pmatrix} u \\ v \end{pmatrix} = D \begin{pmatrix} u \\ v \end{pmatrix} + J_0 \begin{pmatrix} u \\ v \end{pmatrix}, \tag{8}$$

where

$$D = \begin{pmatrix} d_1 \Delta & 0 \\ 0 & d_2 \Delta \end{pmatrix}, \quad J_0 = \begin{pmatrix} \frac{\gamma}{2} - 1 & \frac{\gamma}{2} \\ -\frac{b}{2} & -\frac{b}{2} \end{pmatrix}.$$

Considering the eigenvalue problem

$$L\begin{pmatrix}\Phi_1\\ \Phi_2\end{pmatrix}=\lambda_k\begin{pmatrix}\Phi_1\\ \Phi_2\end{pmatrix}.$$

As such, let

$$\begin{pmatrix}\Phi_1\\ \Phi_2\end{pmatrix}=\sum_{k=0}^{\infty}\begin{pmatrix}a_k\\ b_k\end{pmatrix}\cos(kx),$$

be an eigenfunction about matrix J_k with eigenvalue λ_k, where a_k, b_k are constants. Then, one has

$$\sum_{k=0}^{\infty}(J_k-\lambda_k I)\begin{pmatrix}a_k\\ b_k\end{pmatrix}\cos(kx)=0,$$

where

$$J_k=\begin{pmatrix}\frac{\gamma}{2}-1-d_1k^2 & \frac{\gamma}{2}\\ -\frac{b}{2} & -\frac{b}{2}-d_2k^2\end{pmatrix}.$$

Therefore, we get the following characteristic equation

$$\lambda_k^2-T_k(\gamma)\lambda_k+D_k(\gamma)=0,\quad k\in\mathbb{N}_0=\{0,1,2,\cdots\},\tag{9}$$

where

$$\begin{cases}T_k(\gamma)=-(d_1+d_2)k^2+\frac{\gamma}{2}-\frac{b}{2}-1,\\ D_k(\gamma)=d_1d_2k^4-\left[\left(\frac{\gamma}{2}-1\right)d_2-\frac{b}{2}d_1\right]k^2+\frac{b}{2}.\end{cases}$$

3.1 Turing instability

To yield the occurrence conditions of the Turing instability, we should ensure the positive equilibrium E_* is stable for the local model (4), while it becomes unstable for the diffusive model (3). To this end, we always assume that one of the conclusions (1) and (2) in Theorem 1 is valid. By this way, we immediately have $T_k(\gamma)<0$ for all $k\in\mathbb{N}_0$. Accordingly, we only need to focus on the sign of $D_k(\gamma)$ to seek the conditions of the Turing

instability. Considering the critical condition of the Turing instability $\min_{k\in\mathbb{N}_0\{0\}} D_k(\gamma) = 0$. This gives $\min_{k\in\mathbb{N}_0\{0\}} D_k(\gamma) := -h(\gamma) = 0$, where

$$h(\gamma) = d_2^2\gamma^2 - 2d_2(2d_2 + bd_1)\gamma + (2d_2 - bd_1)^2.$$

Now a direct calculation illustrates that $h(\gamma) = 0$ has two different positive real roots, say γ_1^*, γ_2^*, where

$$\gamma_1^* = \frac{2d_2 + bd_1 - 2\sqrt{2bd_1d_2}}{d_2} > 0, \quad \gamma_2^* = \frac{2d_2 + bd_1 + 2\sqrt{2bd_1d_2}}{d_2} > 0.$$

We claim that $h(\gamma) < 0$ when $\gamma_1^* < \gamma < \gamma_2^*$ and $h(\gamma) > 0$ when $\gamma > \gamma_2^*$ or $0 < \gamma < \gamma_1^*$. As a consequence, one has $D_k(\gamma) > 0$ when $\gamma_1^* < \gamma < \gamma_2^*$ and $D_k(\gamma) < 0$ when $\gamma > \gamma_2^*$ or $0 < \gamma < \gamma_1^*$. It is suggested that the unique positive equilibrium E_* is locally asymptotically stable when $\gamma_1^* < \gamma < \gamma_2^*$ and it is unstable as $\gamma > \gamma_2^*$ or $0 < \gamma < \gamma_1^*$. Now if we treat γ as the Turing instability parameter, the diffusive model (3) may undergo the Turing instability near γ_1^* or γ_2^*. Also, again using $\min_{k\in\mathbb{N}_0\{0\}} D_k(\gamma) = 0$, we get the critical wave number of the Turing instability is $k^2 = k_c^2 = \sqrt{\frac{b}{2d_1d_2}}$.

Based on the analysis above, we build the following.

Theorem 3. *Assume that one of the conclusions (1), (2) in Theorem 1 is valid.*

(1) E_* is locally asymptotically stable when $\gamma_1^* < \gamma < \gamma_2^*$;

(2) E_* is unstable and there exists the Turing instability as $\gamma > \gamma_2^*$ or $0 < \gamma < \gamma_1^*$, where

$$\gamma_1^* = \frac{2d_2 + bd_1 - 2\sqrt{2bd_1d_2}}{d_2} > 0, \quad \gamma_2^* = \frac{2d_2 + bd_1 + 2\sqrt{2bd_1d_2}}{d_2} > 0.$$

3.2 Hopf bifurcation

In what follows, we shall explore the spatial inhomogeneous Hopf bifurcation of the model (3). To this purpose, let $T_k(\gamma) = 0$ for $k \in \mathbb{N}_0/\{0\}$, then we obtain $\gamma := \gamma_k^H = 2(d_1 + d_2)k^2 + b + 2$. Now supposing that $\lambda = \alpha(\gamma) \pm i\omega(\gamma)$ are the eigenvalues of the characteristic equation (9),

then one has

$$\alpha(\gamma)=\frac{T_k(\gamma)}{2},\quad \omega(\gamma)=\frac{\sqrt{4D_k(\gamma)-T_k^2(\gamma)}}{2}. \tag{10}$$

Obviously, if $\gamma:=\gamma_k^H=2(d_1+d_2)k^2+b+2$ for $k\in\mathbb{N}_0/\{0\}$, we have

$$\alpha(\gamma_k^H)=0,\quad \omega(\gamma_k^H)=\sqrt{D_k(\gamma_k^H)}.$$

Now we shall look for some conditions such that $\omega(\gamma_k^H)=\sqrt{D_k(\gamma_k^H)}>0$ is valid. In fact, if $\gamma:=\gamma_k^H=2(d_1+d_2)k^2+b+2$ for $k\in\mathbb{N}_0/\{0\}$, one yields

$$\begin{aligned}D_k(\gamma_k^H)=&d_1d_2k^4-\left[\left(\frac{\gamma_k^H}{2}-1\right)d_2-\frac{b}{2}d_1\right]k^2+\frac{b}{2}\\=&-d_2^2k^4+\frac{b}{2}(d_1-d_2)k^2+\frac{b}{2}.\end{aligned}$$

Let $z=k^2>0$, then $D_k(\gamma_k^H)=0$ has a unique positive real root

$$z=\frac{b(d_1-d_2)+\sqrt{b^2(d_1-d_2)^2+8bd_2^2}}{4d_2^2}>0.$$

Hence, for the spatial inhomogeneous Hopf bifurcation, we take $k=k_H$, where k_H enjoys

$$k_H^2=\begin{cases}\left[\frac{b(d_1-d_2)+\sqrt{b^2(d_1-d_2)^2+8bd_2^2}}{4d_2^2}\right]+1,\ \text{if } D_k([z])\le D_k([z]+1),\\ \left[\frac{b(d_1-d_2)+\sqrt{b^2(d_1-d_2)^2+8bd_2^2}}{4d_2^2}\right],\ \text{if } D_k([z])>D_k([z]+1),\end{cases} \tag{11}$$

where $[\cdot]$ is the integer function. In this fashion, we know that $\omega(\gamma_k^H)=\sqrt{D_k(\gamma_k^H)}>0$ is valid for some $k=k_H\in\mathbb{N}_0/\{0\}$. On the other hand, a straightforward computation gives that

$$\frac{d\mathrm{Re}(\lambda)}{d\gamma}\Big|_{\gamma=\gamma_k^H}=\frac{1}{4}>0.$$

As a result, the model admits the Hopf bifurcation as $\gamma = \gamma_k^H$ for some $k = k_H \in \mathbb{N}_0/\{0\}$.

We establish the following.

Theorem 4. *The diffusive model (3) enjoys the spatial inhomogeneous Hopf bifurcation around* $\gamma := \gamma_k^H = 2(d_1 + d_2)k^2 + b + 2$ *for* $k = k_H$*, where* k_H *has been defined by (11).*

3.3 The direction of the Hopf bifurcation

Define

$$\mathbf{X} = \{(u, v) \in H^2([0, \pi]) \times H^2([0, \pi]) : \\ u_x(0, t) = u_x(\pi, t) = 0 = v_x(0, t) = v_x(\pi, t)\},$$

where $H^2([0, \pi])$ is the standard Sobolev space. Moreover, $D_L := \mathbf{X}_C = \mathbf{X} \oplus i\mathbf{X} = \{a + ib : a, b \in \mathbf{X}\}$. Let L^* be the adjoint operator of the operator L, where L can be found in (8). Making use of a transformation $(u - 1, v - 2) \to (u_1, u_2)$, then model (3) becomes

$$\begin{cases} \frac{\partial U}{\partial t} = L(\gamma)U + F(\gamma, U), \\ \frac{\partial U}{\partial x}(0, t) = \frac{\partial U}{\partial x}(\pi, t) = (0, 0)^T, \end{cases} \tag{12}$$

where $U = (u_1, u_2)^T$, $F(\gamma, U) = (f(\gamma, u_1, u_2), g(\gamma, u_1, u_2))^T$ and

$$L(\gamma) = \begin{pmatrix} d_1\Delta + \frac{\gamma}{2} - 1 & \frac{\gamma}{2} \\ -\frac{b}{2} & d_2\Delta - \frac{b}{2} \end{pmatrix}$$

and

$$F(\gamma, U) = \begin{pmatrix} f(u_1, u_2) - \left(\frac{\gamma}{2} - 1\right) u_1 - \frac{\gamma}{2} u_2 \\ g(u_1, u_2) + \frac{b}{2} u_1 + \frac{b}{2} u_2 \end{pmatrix}.$$

Accordingly, around the Hopf bifurcation threshold $\gamma = \gamma_0^H$, model (12) takes the form

$$\begin{cases} \frac{\partial U}{\partial t} = L(\gamma_0^H)U + F(\gamma_0^H, U), \\ \frac{\partial U}{\partial x}(0,t) = \frac{\partial U}{\partial x}(\pi,t) = (0,0)^T, \end{cases} \tag{13}$$

where

$$L(\gamma_0^H) = \begin{pmatrix} d_1\Delta + \frac{b}{2} & \frac{b+2}{2} \\ -\frac{b}{2} & d_2\Delta - \frac{b}{2} \end{pmatrix}$$

and

$$F(\gamma_0^H, U) = \begin{pmatrix} f(u_1,u_2) - \frac{b}{2}u_1 - \frac{b+2}{2}u_2 \\ g(u_1,u_2) + \frac{b}{2}u_1 + \frac{b}{2}u_2 \end{pmatrix}.$$

Moreover, $F(\gamma_0^H, U)$ can be expressed as follows

$$F(\gamma_0^H, U) = \frac{1}{2}R(U,U) + \frac{1}{6}N(U,U,U) + O(|U|^4),$$

where R and N admit

$$R(U,V) = \begin{pmatrix} R_1(U,V) \\ R_2(U,V) \end{pmatrix}, \quad N(U,V,w) = \begin{pmatrix} N_1(U,V,w) \\ N_2(U,V,w) \end{pmatrix},$$

and

$$\begin{aligned} R_1(U,V) =& a'_{20}u_1v_1 + a'_{11}(u_1v_2 + u_2v_1), \\ R_2(U,V) =& b'_{20}u_1v_1 + b'_{11}(u_1v_2 + u_2v_1), \\ N_1(U,V,w) =& a'_{30}u_1v_1w_1 + a'_{21}(u_1v_1w_2 + u_1v_2w_1 + u_2v_1w_1), \\ N_2(U,V,w) =& b'_{30}u_1v_1w_1 + b'_{21}(u_1v_1w_2 + u_1v_2w_1 + u_2v_1w_1), \end{aligned}$$

with

$$\begin{aligned} a'_{20} = \frac{\gamma_0^H}{2}, \quad a'_{11} = \frac{3\gamma_0^H}{2}, \quad a'_{30} = -\frac{3\gamma_0^H}{4}, \quad a'_{21} = \frac{3\gamma_0^H}{4}, \\ b'_{20} = -\frac{b}{2}, \quad b'_{11} = -\frac{3b}{2}, \quad b'_{30} = \frac{3b}{4}, \quad b'_{21} = -\frac{3b}{4}, \end{aligned}$$

for $U=(u_1,u_2)^T, V=(v_1,v_2)^T, w=(w_1,w_2)^T$ and U,V,w in $H^2([0,\pi])\times H^2([0,\pi])$.

Let

$$q=\begin{pmatrix} q_1 \\ q_2 \end{pmatrix}=\begin{pmatrix} -\frac{b+2i\omega_*}{\gamma_0^H b-(b+2i\omega_*)^2} \\ \frac{b}{\gamma_0^H b-(b+2i\omega_*)^2}, \end{pmatrix}, \quad q^*=\begin{pmatrix} q_1^* \\ q_2^* \end{pmatrix}=\begin{pmatrix} b-2i\omega_* \\ \gamma_0^H \end{pmatrix}.$$

Hence, we can confirm that $\langle L^*(\gamma_0^H)U_1,U_2\rangle=\langle U_1,L(\gamma_0^H)U_2\rangle, L(\gamma_0^H)q=i\omega_* q, L^*(\gamma_0^H)q^*=-i\omega_* q^*, \langle q^*,q\rangle=1$ and $\langle q^*,\overline{q}\rangle=0$, where $\langle\cdot,\cdot\rangle$ is an inner product enjoys $\langle z_1,z_2\rangle=\frac{1}{\pi}\times\int_0^\pi \bar{z_1}^T z_2 dx$ for $z_1\in D_L, z_2\in D_{L^*}$ and $\omega_*=\sqrt{\frac{b}{2}}>0$. In addition, $L^*(\gamma_0^H)$ is given by

$$L^*(\gamma_0^H)=\begin{pmatrix} d_1\Delta+\frac{\gamma_0^H}{2}-1 & -\frac{b}{2} \\ \frac{\gamma_0^H}{2} & d_2\Delta-\frac{b}{2} \end{pmatrix}=\begin{pmatrix} d_1\Delta+\frac{b}{2} & -\frac{b}{2} \\ \frac{b}{2}+1 & d_2\Delta-\frac{b}{2} \end{pmatrix}.$$

Benefiting from [16], one has $\mathbf{X}=\mathbf{X}^c\oplus\mathbf{X}^s$ with $\mathbf{X}^c:=\{zq+\overline{zq}|z\in\mathbb{C}\}$ and $\mathbf{X}^s=\{w\in\mathbf{X}|\langle q^*,w\rangle=0\}$, where $z=\langle q^*,U\rangle$ with $U=(u_1,u_2)^T$. Consequently, for any $U\in\mathbf{X}$, there exists $z\in\mathbb{C}$ and $w=(w_1,w_2)\in\mathbf{X}^s$ such that

$$\begin{pmatrix} u_1 \\ u_2 \end{pmatrix}=zq+\bar{z}\bar{q}+\begin{pmatrix} w_1 \\ w_2 \end{pmatrix}.$$

In this fashion, model (13) takes the form

$$\begin{cases} \frac{dz}{dt}=i\omega_* z+\langle q^*,\widetilde{f}\rangle, \\ \frac{dw}{dt}=L(\gamma_0^H)w+K(z,\overline{z},w), \end{cases} \tag{14}$$

where

$$\widetilde{f}=F(zq+\bar{z}\bar{q}+w,\gamma_0^H), \quad K(z,\overline{z},w)=\widetilde{f}-\langle q^*,\widetilde{f}\rangle q-\langle\bar{q}^*,\widetilde{f}\rangle\overline{q}.$$

Some straightforward calculations give

$$\widetilde{f}=\frac{1}{2}R(q,q)z^2+R(q,\overline{q})z\overline{z}+\frac{1}{2}R(\overline{q},\overline{q})\overline{z}^2+O(|z|^3,|z|\cdot|w|,|w|^2),$$

$$\begin{aligned}\langle q^*, \widetilde{f}\rangle =&\frac{1}{2}\langle q^*, R(q,q)\rangle z^2 + \langle q^*, R(q,\overline{q})\rangle z\overline{z}\\ &+ \frac{1}{2}\langle q^*, R(\overline{q},\overline{q})\rangle \overline{z}^2 + O(|z|^3, |z|\cdot|w|, |w|^2),\\ \langle \overline{q}^*, \widetilde{f}\rangle =&\frac{1}{2}\langle \overline{q}^*, R(q,q)\rangle z^2 + \langle \overline{q}^*, R(q,\overline{q})\rangle z\overline{z}\\ &+ \frac{1}{2}\langle \overline{q}^*, R(\overline{q},\overline{q})\rangle \overline{z}^2 + O(|z|^3, |z|\cdot|w|, |w|^2).\end{aligned}$$

Consequently, one yields

$$K(z,\overline{z},w) = \frac{1}{2}z^2K_{20} + z\overline{z}K_{11} + \frac{1}{2}\overline{z}^2K_{02} + O(|z|^3, |z|\cdot|w|, |w|^2),$$

where

$$\begin{aligned}K_{20} &= R(q,q) - \langle q^*, R(q,q)\rangle q - \langle \overline{q}^*, R(q,q)\rangle \overline{q},\\ K_{11} &= R(q,\overline{q}) - \langle q^*, R(q,\overline{q})\rangle q - \langle \overline{q}^*, R(q,\overline{q})\rangle \overline{q},\\ K_{02} &= R(\overline{q},\overline{q}) - \langle \overline{q}^*, R(\overline{q},\overline{q})\rangle q - \langle \overline{q}^*, R(\overline{q},\overline{q})\rangle \overline{q}.\end{aligned}$$

Some computations imply that

$$K_{20} = K_{11} = K_{02} = (0,0)^T.$$

Hence, we get

$$K(z,\overline{z},w) = O(|z|^3, |z|\cdot|w|, |w|^2).$$

By employing [16], we deduce that system (14) has a center manifold as below

$$w = \frac{1}{2}z^2w_{20} + z\overline{z}w_{11} + \frac{1}{2}\overline{z}^2w_{02} + O(|z|^3).$$

It is noticed that

$$Lw + K(z,\overline{z},w) = \frac{dw}{dt} = \frac{\partial w}{\partial z}\frac{dz}{dt} + \frac{\partial w}{\partial \overline{z}}\frac{d\overline{z}}{dt}.$$

As such, we have

$$w_{20} = [2i\omega_* - L(\gamma_0^H)]^{-1}K_{20} = (0,0)^T,$$

$$w_{11} = -L^{-1}(\gamma_0^H)K_{11} = (0,0)^T,$$
$$w_{02} = [-2i\omega_* - L(\gamma_0^H)]^{-1}K_{02} = (0,0)^T.$$

Consequently, the diffusive model (3) restricts to the center manifold is

$$\frac{dz}{dt} = i\omega_* z + \langle q^*, \widetilde{f}\rangle = i\omega_* z + \sum_{2\le i+j\le 3} \frac{g_{ij}}{i!j!} z^i \overline{z}^j + O(|z|^4), \tag{15}$$

where

$$g_{02} = \langle q^*, R(\overline{q},\overline{q})\rangle, \quad g_{20} = \langle q^*, R(q,q)\rangle, \quad g_{11} = \langle q^*, R(q,\overline{q})\rangle,$$
$$g_{21} = 2\langle q^*, R(w_{11},q)\rangle + \langle q^*, R(w_{20},\overline{q})\rangle + \langle q^*, N(q,q,\overline{q})\rangle = \langle q^*, N(q,q,\overline{q})\rangle.$$

Now rewriting (15) as the Poincaré normal form

$$\frac{dz}{dt} = (\alpha(\gamma) + i\omega(\gamma))z + z\sum_{j=1}^{N} \tau_j(\gamma)(z\overline{z})^j, \tag{16}$$

where z is a complex variable and $\tau_j(\gamma)$ are coefficients. By computing, we get

$$\tau_1(\gamma) = \frac{g_{20}g_{11}[3\alpha(\gamma) + i\omega(\gamma)]}{2[\alpha^2(\gamma) + \omega^2(\gamma)]} + \frac{|g_{11}|^2}{\alpha(\gamma) + i\omega(\gamma)} + \frac{g_{21}}{2} + \frac{|g_{02}|^2}{2[\alpha(\gamma) + 3i\omega(\gamma)]}.$$

It is noticed that $\alpha(\gamma_0^H) = 0$ and $\omega(\gamma_0^H) = \omega_* > 0$, so we have

$$\begin{aligned}\tau_1(\gamma_0^H) =& \frac{g_{20}g_{11}i}{2\omega_*} + \frac{|g_{11}|^2}{i\omega_*} + \frac{g_{21}}{2} + \frac{|g_{02}|^2}{6i\omega_*} \\ =& \frac{i}{2\omega_*}\left(g_{20}g_{11} - 2|g_{11}|^2 - \frac{1}{3}|g_{02}|^2\right) + \frac{g_{21}}{2}.\end{aligned}$$

It gives

$$\mathrm{Re}\{\tau_1(\gamma_0^H)\} = -\frac{1}{2\omega_*}\left(\mathrm{Re}\{g_{20}\}\mathrm{Im}\{g_{11}\} + \mathrm{Im}\{g_{20}\}\mathrm{Re}\{g_{11}\}\right) + \frac{1}{2}\mathrm{Re}\{g_{21}\}.$$

By computation, one yields

$$g_{20} = \overline{q}_1^*(a'_{20}q_1^2 + 2a'_{11}q_1q_2) + \overline{q}_2^*(b'_{20}q_1^2 + 2b'_{11}q_1q_2),$$

$$g_{11} = \overline{q}_1^*[a'_{20}q_1\overline{q}_1 + a'_{11}(q_1\overline{q}_2 + q_2\overline{q}_1)] + \overline{q}_2^*[b'_{20}q_1\overline{q}_1 + b'_{11}(q_1\overline{q}_2 + q_2\overline{q}_1)],$$
$$g_{21} = \overline{q}_1^*[a'_{30}q_1^2\overline{q}_1 + a'_{21}(q_1^2\overline{q}_2 + 2q_2q_1\overline{q}_1)] + \overline{q}_2^*[b'_{30}q_1^2\overline{q}_1 + b'_{21}(q_1^2\overline{q}_2 + 2q_2q_1\overline{q}_1)].$$

We have the following result.

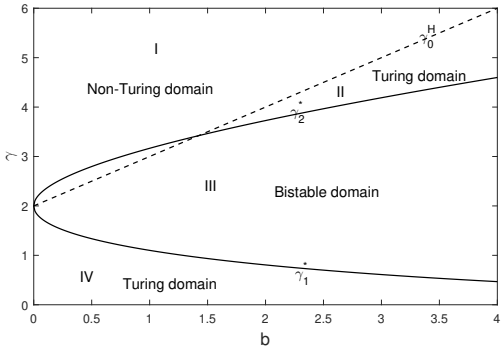

Figure 4. Stability diagram of E_* in the plane of $b - \gamma$.

Theorem 5. *For $d_1 > 0$ and $d_2 > 0$, the modified Brusselator model (3) undergoes the Hopf bifurcation around $\gamma = \gamma_0^H$. Moreover,*

(1) the Hopf bifurcation is supercritical if $Re\{\tau_1(\gamma_0^H)\} < 0$ and the periodic solution induced by the Hopf bifurcation is stable if $Re\{\tau_1(\gamma_0^H)\} < 0$;

(2) the Hopf bifurcation is subcritical if $Re\{\tau_1(\gamma_0^H)\} > 0$ and the periodic solution induced by the Hopf bifurcation is stable if $Re\{\tau_1(\gamma_0^H)\} > 0$.

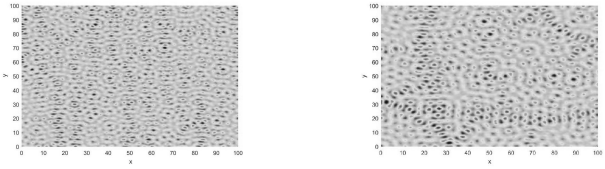

(a) $\gamma = 2.32$ (b) $\gamma = 2.34$

Figure 5. Self-organization pattern induced by the Turing instability when fixing $b = 0.5, d_1 = 0.2, d_2 = 8.5$, while taking different γ. (a): $\gamma = 2.32$; (b): $\gamma = 2.34$.

4 Numerical simulations

4.1 Self-organization pattern induced by the Turing instability

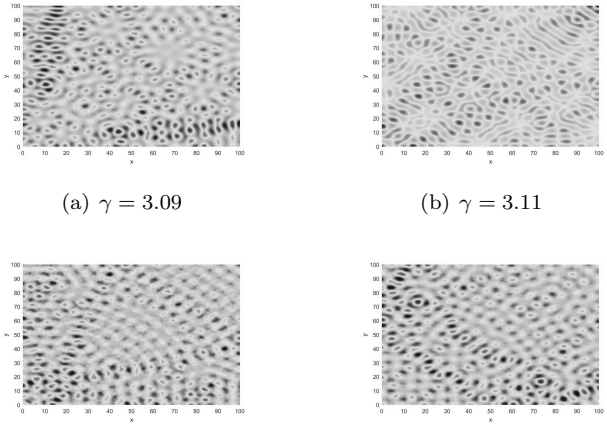

(a) $\gamma = 3.09$ (b) $\gamma = 3.11$

(c) $\gamma = 3.45$ (d) $\gamma = 3.50$

Figure 6. Self-organization pattern induced by the Turing instability when fixing $b = 2, d_1 = 0.2, d_2 = 8.5$, while taking different γ. (a): $\gamma = 3.09$; (b): $\gamma = 3.11$; (c): $\gamma = 3.45$; (d): $\gamma = 3.50$.

In this subsection, we perform some self-organization patterns by using numerical simulations. Firstly, benefiting from Theorem 1 and Theorem 3, we give a stability classification of the unique positive equilibrium E_*. In Fig. 4, the parameter plane $b-\gamma$ is divided into four domains by the Turing instability critical curves γ_1^*, γ_2^* and the Hopf bifurcation curve γ_0^H, say I, II, III, and IV, respectively. In the domain I, we know that equilibrium E_* is unstable for the local model (4) due to $\gamma > \gamma_0^H$. Consequently, it is the non-Turing domain. In the domain II, clearly, one claims that $\gamma_2^* < \gamma < \gamma_0^H$. Accordingly, equilibrium E_* is locally asymptotically stable for the local model (ODEs) (4), and it becomes unstable for the model (3) (PDEs), so this domain is the Turing domain. In a similar fashion, we claim that IV is the Turing domain. Next, in the domain III, we find that $\gamma_1^* < \gamma < \gamma_2^* (< \gamma_0^H)$ is valid. This implies that the equilibrium E_* is locally

asymptotically stable for the ODEs and it is also stable for the PDEs. As such, we think that III is a bi-stable domain. Consequently, we should restrict the parameters $(b, \gamma) \in II$ or $(b, \gamma) \in IV$ for the self-organization patterns of the modified Brusselator model (3).

Now we are especially interested in the self-organization patterns in 2D space for the modified Brusselator model (3) by employing two-dimensional finite-difference method. Accordingly, we fix the bounded domain $\Omega = [0, 100] \times [0, 100]$, the time step length is $\Delta t = 0.25$, and the spatial step length is $\Delta h = 0.5$. Also, the initial data we choose is

$$u(x, y, 0) = u_* - 0.0015 \times \zeta_*, \quad v(x, y, 0) = v_* - 0.0015 \times \zeta_*,$$

where ζ_* is the uniformly random perturbation.

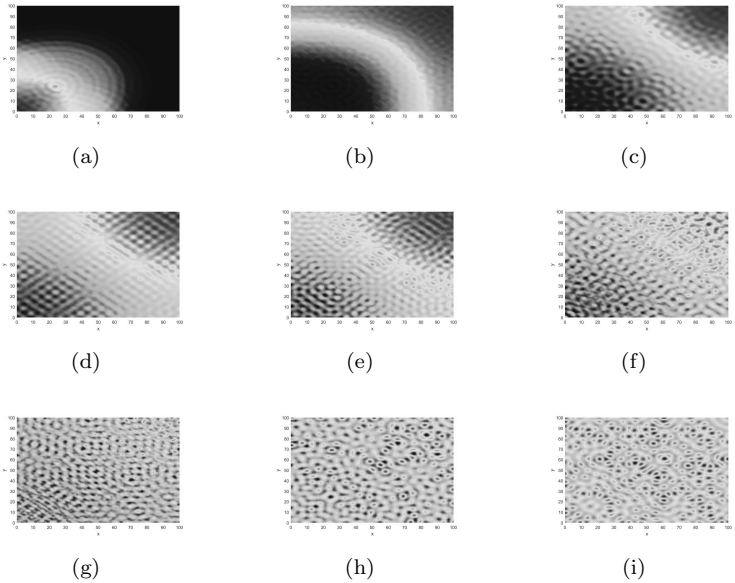

(a) (b) (c)

(d) (e) (f)

(g) (h) (i)

Figure 7. Self-organization pattern evolutions of the model (3) with $b = 2, d_1 = 0.2, d_2 = 8.5$, and $\gamma = 3.09$.

Firstly, let us take $b = 0.5, d_1 = 0.2, d_2 = 8.5$, then one obtains $\gamma_1 = b + 2 - 2\sqrt{2b} = 0.5, b + 2 = 2.5, \gamma_1^* = 1.7050$, and $\gamma_2^* = 2.3186$. Then by using (2) in Theorem 1, we know that the unique positive equilibrium E_*

Table 1. Values of parameters.

b	d_1	d_2	γ	γ_0^H	$\mathrm{Re}\{\tau_1(\gamma_0^H)\}$	Figure
0.25	0.20	1.50	2.25	2.25	-0.4219	Fig. 9(a)
0.50	0.20	1.50	2.50	2.50	-0.1406	Fig. 9(b)
0.75	0.20	1.50	2.75	2.75	-0.0469	Fig. 9(c)
0.90	0.50	1.50	2.90	2.90	-0.0156	Fig. 9(d)

is locally asymptotically stable for the non-diffusive model (4). Also, by virtue of (2) in Theorem 3, we claim that there exists the Turing instability for the diffusive Brusselator-type model (3) when $\gamma \in (2.3186, 2.5)$. Our numerical simulation checks the validity of this aspect. We can observe that there is the spatial pattern formation of the model (3) in the bounded domain Ω with the different values of the control parameter γ, see Fig. 5.

Figure 5 gives the pattern formation of the diffusive Brusselator model (3) for $0 < b < 1$. In what follows, we want to exhibit the self-organization patterns of the model (3) when $b \geq 1$ with different control parameters γ. For this purpose, one chooses $b = 2, d_1 = 0.5, d_2 = 8.5$, then one obtains $b + 2 = 4, \gamma_1^* = 1.1475$, and $\gamma_2^* = 3.0878$. Then by employing (2) in Theorem 1, we know that the unique positive equilibrium E_* is locally asymptotically stable for the non-diffusive model (4). Moreover, from (2) in Theorem 3, we deduce that there is the Turing instability for the diffusive Brusselator-type model (3) when taking $\gamma \in (3.0878, 4)$. To display the self-organization patterns of model (3), we respectively treat $\gamma = 3.09, 3.11, 3.45$, and 3.5, we can observe that there is the spatial pattern formation of the model (3) in the bounded domain Ω, see Fig. 6. Figure 7 gives the detailed self-organization pattern evolutions when fixing the control parameter $\gamma = 3.09$ with different moments. Hence, the theoretical predictions are confirmed by the numerical experiments, and there are self-organization patterns in the model (3).

4.2 Periodic solution induced by the Hopf bifurcation

In this subsection, let us check the validity of Theorem 5. In fact, we mainly want to display the stable periodic solution bifurcated from the supercritical Hopf bifurcation. To do so, we fix the diffusion coefficients $d_1 =$

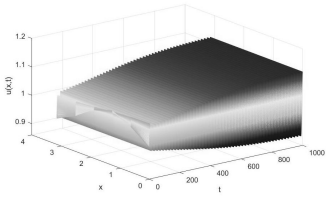

(a)

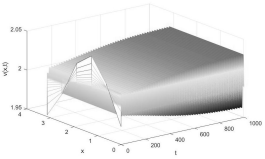

(b)

Figure 8. Stable periodic solution emerges in the model (3) with $b = 0.2, d_1 = 0.2, d_2 = 1.5$, and $\gamma = 2.2$. Initial data are $u_0(x) = 1 - 0.02\cos(x)$ and $u_0(x) = 2 - 0.02\cos(x)$.

$0.2, d_2 = 1.5$ and parameter $b = 0.2$. Then we obtain $q_1 = -0.7906i, q_2 = 0.2273 + 0.0719i, q_1^* = 0.2 - 0.6325i, q_2^* = 2.2, g_{20} = 0.7500 - 0.1976i, g_{11} = 0.1976i, g_{21} = -0.6562 + 0.1482i$. So we obtain $\mathrm{Re}\{g_{20}\} = 0.75, \mathrm{Re}\{g_{11}\} = 0, \mathrm{Im}\{g_{11}\} = 0.1976, \mathrm{Im}\{g_{20}\} = -0.1976, \mathrm{Re}\{g_{21}\} = -0.6562$, and $\gamma_0^H = 2.2$. These give that $\mathrm{Re}\{\tau_1(\gamma_0^H)\} = -0.5625 < 0$. Therefore, by employing (1) in Theorem 5, we know that there is the stable periodic solution. Our numerical simulations confirm this theoretical prediction, see Fig. 8. Finally, Fig. 9 shows the stable periodic solutions with different parameter values of the Hopf bifurcation thresholds $\gamma = \gamma_0^H$ and we organize the specific parameter values in Table 1.

5 Conclusions

In this paper, we study the Hopf bifurcation and self-organization pattern of a modified Brusselator model. For the local model (4), we investigate the types and stability of the unique positive equilibrium E_*. It is found

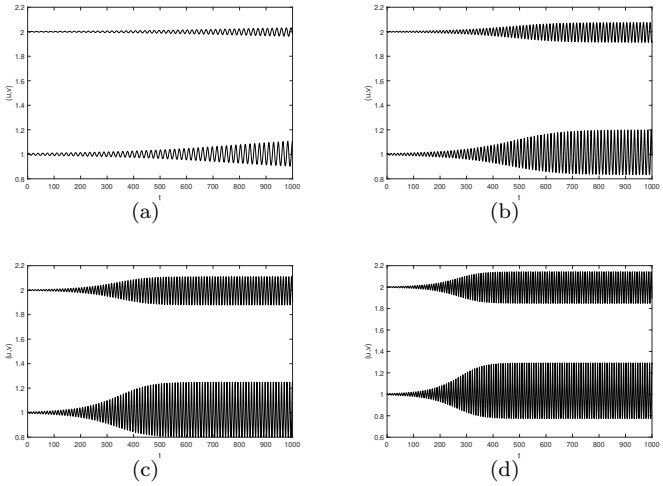

Figure 9. Stable periodic solution bifurcated from the Hopf bifurcation. (a): $b = 0.25, d_1 = 0.20, d_2 = 1.50, \gamma = 2.25$; (b): $b = 0.50, d_1 = 0.20, d_2 = 1.50, \gamma = 2.5$; (c): $b = 0.75, d_1 = 0.20, d_2 = 1.50, \gamma = 2.75$; (d): $b = 0.90, d_1 = 0.50, d_2 = 1.50, \gamma = 2.9$; Initial data are $u_0(x) = 1 - 0.02\cos(x)$ and $u_0(x) = 2 - 0.02\cos(x)$.

that equilibrium E_* may be node, focus, or center, see Theorem 1. If it is a center, then the local model (4) may undergo the Hopf bifurcation, and it is the supercritical type by using the first Lyapunov number, see Theorem 2. We also recommend some known results about Hopf bifurcation for the delayed models, see Refs. [21–24]. In what follows, we focus on the spatial dynamics of the diffusive Brusselator model (3). By direct analysis, we give the occurrence conditions of the Turing instability and spatial inhomogeneous Hopf bifurcation, see Theorem 3 and Theorem 4, respectively. It is noticed that there is the periodic solution bifurcated from the Hopf bifurcation. Thereby, one adopts the center manifold reduction and normal form theory to determine the stability of the periodic solution. The stable and unstable periodic solution can be classified, see Theorem 5. Numerical simulations confirm the validity of our theoretical results. In this fashion, the self-organization patterns induced by the Turing instability and periodic solutions bifurcated from the Hopf bifurcation

with different parameter values are displayed, see Figs. 5-7 and Figs. 8-9, respectively. Chemically, the Hopf bifurcation implies that there is a natural phenomenon that appears cyclical behavior in reaction progress. Of course, we can avoid such behavior by adjusting the control parameter γ. On the other hand, the self-organization patterns reveal the spatial oscillation phenomenon of the model. Generally, this phenomenon is caused by the movement of chemical reactants. Therefore, the spatial oscillation behavior could be controlled by regulating the movement rates of the chemical reactants. Overall, our theoretical predictions and numerical results illustrate that the modified Brusselator model admits wealthy temporal and spatial dynamic profiles. More dynamic profiles of such a modified Brusselator model will be further considered.

***Acknowledgment*:** The authors express their sincere thanks to the anonymous reviewers for their comments on revisions. This work was supported by the China Postdoctoral Science Foundation (No. 2021M701118).

References

[1] R. Asheghi, Stability and Hopf bifurcation analysis of a reduced Gierer-Meinhardt model, *Int. J. Bifur. Chaos* **31** (2021) #2150149.

[2] M. X. Chen, T. Wang, Qualitative analysis and Hopf bifurcation of a generalized Lengyel-Epstein model, *J. Math. Chem.* **61** (2023) 166–192.

[3] U. F. Muntari, T.Sengül, Dynamic transitions and Turing patterns of the Brusselator model, *Math. Meth. Appl. Sci.* **45** (2022) 9130–9151.

[4] T. Wong, M. J. Ward, Spot patterns in the 2-D Schnakenberg model with localized heterogeneities, *Stud. Appl. Math.* **146** (2021) 779–833.

[5] M. X. Chen, R. C. Wu, L. P. Chen, Pattern dynamics in a diffusive Gierer-Meinhardt model, *Int. J. Bifur. Chaos* **30** (2020) #2030035.

[6] Y. Ishii, Stability analysis of spike solutions to the Schnakenberg model with heterogeneity on metric graphs, *J. Nonlin. Sci.* **32** (2022) #11.

[7] S. Bilazeroglu, H. Merdan, L. Guerrini, Hopf bifurcation of a Lengyel-Epstein model involing two discrete time delays, *Discr. Contin. Dyn. Sys.* **15** (2022) 535–554.

[8] Q. Din, U. Saeed, Stability, discretization, and bifurcation analysis for a chemical reaction system, *MATCH Commun. Math. Comput. Chem.* **90** (2023) 151–174.

[9] A. Cassani, A. Monteverde, Marco Piumetti, Belousov-Zhabotinsky type reactions: the nonlinear behavior of chemical systems, *J. Math. Chem.* **59** (2021) 792–826.

[10] I. Prigogene, R. Lefever, Symmetry breaking instabilities in dissipative system II, *J. Chem. Phys.* **48** (1968) 1665–1700.

[11] Q. Bie, Pattern formation in a general two-cell Brusselator model, *J. Math. Anal. Appl.* **376** (2011) 551–564.

[12] K. J. Brown, F. A. Davidson, Global bifurcation in the Brusselator system, *Nonlin. Anal.* **24** (1995) 1713–1725.

[13] I. Rozada, S. J. Ruuth, M. J. Ward, The stability of localized spot patterns for the Brusselator on the sphere, *SIAM J. Appl. Dyn. Sys.* **13** (2014) 564–627.

[14] M. X. Chen, R. C. Wu, L. Chen, Turing-Turing and Turing-Hopf bifurcations in a general diffusive Brusselator model, *ZAMM Z. Ang. Math. Mech.* (2023) doi: 10.1002/zamm.201900111.

[15] L. Perko, *Differential Equations and Dynamical Systems*, Springer, New York, 2001.

[16] B. D. Hassard, N. D. Kazarinoff, Y. H. Wan, *Theory and Applications of Hopf Bifurcation*, Cambridge Univ. Press, Cambridge, 1981.

[17] M. X. Chen, R. C. Wu, X. H. Wang, Non-constant steady states and Hopf bifurcation of a species interaction model, *Commun. Nonlin. Sci. Num. Sim.* **116** (2023) #106846.

[18] Y. L. Song, Y. H. Peng, X. F. Zou, Persistence, stability and Hopf bifurcation in a diffusive ratio-dependent predator-prey model with delay, *Int. J. Bifur. Chaos* **24** (2014) #1450093.

[19] Y. Li, J. L. Wang, X. J. Hou, Stripe and spot patterns for the Gierer-Meinhardt model with saturated activator production, *J. Math. Anal. Appl.* **449** (2017) 1863–1879.

[20] C. Y. Zhang, R. C. Wu, M. X. Chen, Hopf bifurcation in a delayed predator-prey system with general group defense for prey, *J. Appl. Anal. Comput.* **11** (2021) 810–840.

[21] C. D. Huang, J. Y. Tang, Y. T. Niu, J. Cao, Enhanced bifurcation results for a delayed fractional neural network with heterogeneous orders, *Physica A* **526** (2019) #121014.

[22] C. D. Huang, J. Wang, X. P. Chen, J. Cao, Bifurcations in a fractional-order BAM neural network with four different delays, *Neural Networks* **141** (2021) 344–354.

[23] C. J. Xu, W. Zhang, C. Aouiti, Z. Liu, L. Yao, Bifurcation insight for a fractional-order stage-structured predator-prey system incorporating mixed time delays, *Math. Meth. Appl. Sci.* (2023) doi: `10.1002/mma.9041`.

[24] C. J. Xu, D. Mu, Z. X. Liu, Y. Pang, M. Liao, C. Aouiti, New insight into bifurcation of fractional-order 4D neural networks incorporating two different time delays, *Commun. Nonlin. Sci. Num. Sim.* **118** (2023) #107043.